Earthquake Geotechnical Engineering for Protection and Development of Environment and Constructions – Silvestri & Moraci (Eds)
© 2019 Associazione Geotecnica Italiana, Rome, Italy, ISBN 978-0-367-14328-2

Study on early recognition of geohazards based on dynamic amplification and deformation characteristics

Y. Tang, A.L. Che & R.J. Zhu
Shanghai Jiaotong University, Shanghai, China

X.H. Shuai
China Earthquake Networks Center, Beijing, China

ABSTRACT: Earthquake-triggered geohazards can be one of the main reasons for a large number of casualties and property losses. In earthquake-prone areas, early recognition methods of geohazards are very important. For an extensive loess landslide disaster, a typical slope in the Loess Plateau-Cuiying Mountain was selected as the research object, and a series of field tests was performed. The method of microtremor observation was used to evaluate the amplification characteristics, based on which the method of Newmark sliding block was used to analyze the stability of the slope under the Minxian-Zhangxian Ms 6.6 earthquake. The calculation results reveal that the slope has a risk of instability in areas 1, 2, and 3. UAV aerial photography is used to analyze the deformation characteristics and recognize the sliding mode as multistage sliding. With the dynamic amplification and deformation characteristics, the early recognition of earthquake landslide disasters can be achieved.

1 INTRODUCTION

Loess is porous and weakly cemented quaternary sediment that is mainly composed of silt, less sand and clay. Therefore, it has high seismic vulnerability. According to the statistics, there are more than 40,000 new and old landslides in eastern Gansu, causing great casualties and property losses (Zhao et al. 2016). The Loess Plateau is the main distribution area of loess in China and has complex topography and geomorphology (Zhang et al. 2014). The neotectonics activities in the Loess Plateau are strong and result in the frequent occurrence of strong earthquakes. Such earthquakes will induce a large number of loess landslides (Pu et al. 2016). For example, many slope disasters were caused by the Wenchuan Ms 8.0 earthquake on May 12, 2008 in the southern Gansu Province (Xing et al. 2010). Many loess landslides occurred because of the Minxian-Zhangxian Ms. 6.6 earthquake on July 22, 2013, the well-known one was Yongguang Village landslide, which caused 12 deaths (Xu et al. 2013).

The reasons that loess landslides cause such heavy damage are as follows: First, the loess slope has long-term stability problems under the action of external forces such as earthquakes or rainfall. Second, it is difficult to accurately recognize or predict landslides with potential hazards (Huang et al. 2004). At present, in addition to the management of known disaster points, the active and rapid recognition of landslide disasters is very important. There are many methods to identify landslide hazards. Zhang et al. (2016) conducted the recognition of landslide by using object-oriented classification methods and the data of Geoeye-1 and digital elevation model (DEM) were used as raw data. Unmanned Aerial Vehicles (UAVs) have been the main tool to recognize the deformation; they are used to collect time series of high-resolution images and identify and extract the landslide scarp data (Turner et al. 2015, AlRawabdeh et al. 2016). The geographic information system (GIS) and InSAR technology can be used to study the deformation of the slopes over a long period (Kritikos et al. 2015, Sun et al. 2015). The early identification studies are mainly based on the deformation characteristics of

the slope. In earthquake-prone areas, the dynamic amplification characteristic is also essential to the slope stability. FEM analyses and shaking-table tests are widely recognized as suitable methods to obtain the propagation characteristics of the seismic wave field, dynamic evolution and failure mechanism. Many conclusions have been summarized, e.g., the slope has an amplification effect on the earthquake acceleration. When the soil body is damaged, the slope body displacement will also be enlarged with the increase in earthquake duration time (Zhu et al. 2018, Roy et al. 2016).

Aiming at the early recognition of geohazards in the Loess Plateau, Cuiying Mountain is selected as the study area because it is a typical loess landslide, and several research teams have conducted long-term monitoring in this area, then we conducted a series of observations. Based on the dynamic amplification and deformation characteristics, the method of microtremor observation is used to evaluate the amplification characteristics, based on which the stability of the slope is analyzed using the Newmark sliding block method. UAV aerial photography is used to analyze the deformation characteristics and recognize the sliding mode.

2 CASE STUDY

Cuiying Mountain is located at Lanzhou University Yuzhong Campus, which is approximately 50 km from Lanzhou City. The location is shown in Fig. 1. The elevation of the mountain is approximately 2,000 m, and the mountain is located in the northwest inland with a continental climate. Specifically, it belongs to the mid-temperate semiarid climate. Under natural conditions, atmospheric precipitation is the only source of groundwater in this area. In addition, considering that Gansu Province is an earthquake-prone region, this region is located in the central-northern portion of the Sorth-Nouth Seismic Belt, and the tectonic is complex. There are many active fault zones in both the boundary and internal areas, including the Eastern Kunlun, Bailongjiang and West-Qinling Faults. Historically, strong earthquakes frequently occurred, as shown in Fig. 2. In particular, earthquakes above Ms 5.0 have occurred in the region in the past, including the Haiyuan 8.5 earthquake on December 16, 1920, 200 km from Cuiying Mountain, which killed 280,000 people, and Minxian-Zhangxian Ms 6.6 earthquake, which was 250 km from Cuiying Mountain.

The mountain is a typical loess landslide in the Loess Plateau with a slope of approximately 20 degrees and a length of approximately 250 m, as shown in Fig. 3a. The slope has less vegetation, and there are many different sizes of loess sinkholes and partial collapses in the slope. Professor Fanyu Zhang team conducted long-term monitoring in the slope, which reveals that the slope has undergone certain deformation due to earthquakes, rainfall, snowmelt and other factors. According to the drilling data in Cuiying Mountain, we can obtain the soil structure,

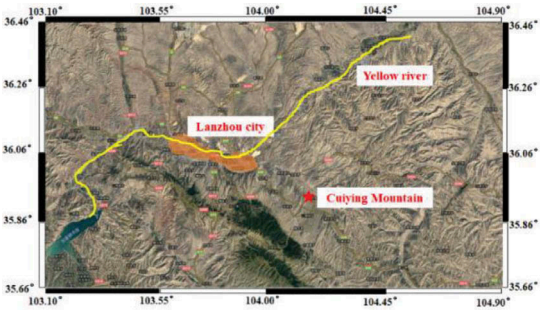

Figure 1. Location of Cuiying Mountain

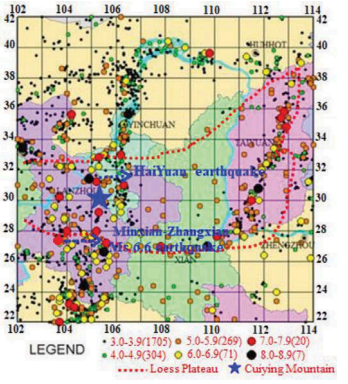

Figure 2. Seismic distribution on the Loess Plateau

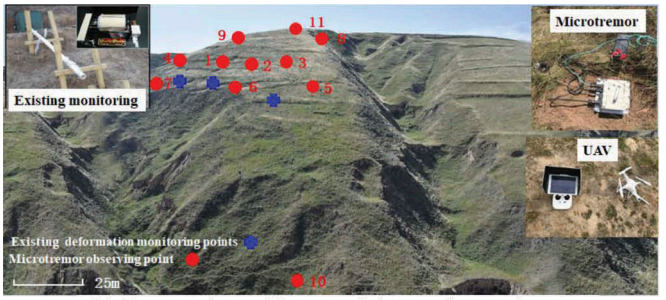

(a) Topography and layout of observation equipment

depth	Soil property	Standard penetration compaction number N	Shear wave velocity V_S	corresponding depths	Ages
0m	Sandy loess	5.0	200	2.0-2.4m	alQ_4
		6.0	210	4.4-5.8m	
		11.0	240	6.7-8.1m	
		14.0	255	9.0-10.4m	
		15.0	260	12.4-14.8m	
		15.0	260	16.5-18.1m	
		17.0	264	19.7-21.1m	
		19.0	275	23.1-24.6m	
		21.0	280	26.2-27.1m	
33m		24.0	300	28.3-30.2m	
		24.0	300	32.1-32.8m	
	Circular gravel				alQ_4
50m					

(b) Geological data

Figure 3. Overview of the study area

as shown in Fig. 3b. The soil samples at various locations show that the 33-m soil layer in the upper part of the mountain is sandy loess at the age of alQ_4. The amount of standard penetration compaction is 5-24, and the corresponding depths are shown in Fig. 3b. The shear wave velocity is 200-300, which can be used to calculate the soil thickness. The lower part is circular gravel mainly composed of quartzite and sandstone, and the thickness is approximately 20 m.

3 FIELD TESTS

At the scene, eleven points were selected to perform the microtremor observation, and a region of approximately 90,000 m^2 was measured by UAV aerial photography. Using the microtremor as a passive source to evaluate the amplification effect of the slope and with the orthophoto data and digital elevation model obtained by UAV aerial photography, we could evaluate the deformation characteristics.

3.1 *Microtremor observation*

Even if there is no earthquake, there will be slight vibration on the ground surface where the amplitude is approximately 10^{-8} cm on the bedrock in the quiet mountain and 10^{-4} cm in the city and the period is 0.05~10.00 sec, which is called microtremor. The generally considered that the causes of microtremor are transportation, machinery operation and other human activities, or from deep formations; weather changes; river, lake or ocean waves; or other natural excitations. It is well known that the microtremor observation is one of the most convenient methods to investigate the dynamic characteristics of the surface ground. On this basis, this paper will consider the microtremor as a passive source to test and evaluate the amplification characteristics of the slope.

The measuring equipment consists of a type of handy seismometer (CV-374AV; distinguish ability: 16 Bit; frequency range: 0~70 Hz) and a three-component high-sensitive detector (VSE-15D velocity detector, which has a natural period in one second). The records of two horizontal components (EW and NS) and a vertical component (UD) with a short-period microtremor were obtained. Eleven observation points were measured and arranged at various locations from the bottom to the top on the surface of the slope, as shown in Fig. 3a. The interference of human activities should be avoided during the investigation, and the sites should be as flat as possible. Because the test was performed on the slope surface, we had to use shovels to flatten the surface of each measuring point to ensure that the natural ground was flat and well-compacted before setting the seismometer. The microtremor data of each point were continuously recorded for approximately 0.5-1.0 h at a sampling frequency of 200 Hz.

To ensure good resolution, we used a 300 s time window to cut the remaining data into time segments. The average amplitude and deviation of each segment were analyzed, and all noisy segments were discarded. The time window with a 10% smooth taper was finely designed to

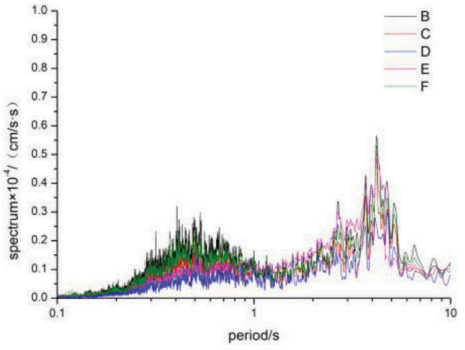

Figure 4. Five segments of spectrum in the horizontal direction of point 4

reduce its effect on the spectrum estimated. The power spectrum of each segment was calculated by fast Fourier transform (FFT). Then, to evaluate the horizontal amplification characteristics of slope, the concept of two horizontal components (EW and NS) average was used to evaluate the horizontal spectrum of slope, and the following formula was used to calculate the horizontal spectrum.

$$a_h = \sqrt{EW \times NS} \tag{1}$$

where a_h is the spectrum in the horizontal direction.

Fig. 4 shows the calculated Fourier spectrum of the velocity in the horizontal directions of point 4; the plots show clear similarities among the five segments. The spectrum always has dominant maxima at short periods (<0.50 sec) that correspond to the main peak in the Fourier spectrum of the velocity. Furthermore, the general decay of the Fourier spectrum of the velocity toward long periods (>1.30 sec) is visible in the spectra. The main peaks of the obtained spectrum are at approximately 0.30-0.50 sec and 1.30-1.50 sec. Those periods are considered as the natural frequency under small shear strain and are closely related with the nature of the ground. Combining with a quarter-wavelength criterion and the shear wave velocity, the dominant frequency of the topsoil in this area is approximately 2.00 Hz. The predominant period of 0.30-0.50 sec is considered as the dynamic characteristic of the soil layer, and the corresponding spectrum calculated from the average of all five segments of each measuring point is summarized in Table 1.

3.2 *UAV aerial photography*

Based on the DJI phantom 4 four-axis aerial survey UAV and PhotoScan software, the data acquisition of the surface image of Cuiying Mountain was performed. The aerial photography directly acquires the image data of the measurement area, which is a direct projection of real objects, and records the color texture and spectral information of different objects in the scene. Fig. 5a shows the entire orthophoto data of the study area, which can be used to analyze the location of the loess sinkhole and surface terrain. The digital elevation model (DEM) is generated by PhotoScan software and ArcGIS, as shown in Fig. 5b. The information of the

Table 1. Predominant period and spectrum values of each point

Monitoring point	1	2	3	4	5	6	7	8	9	10	11
period/s	0.41	0.11	0.40	0.39	0.42	0.42	0.43	0.33	0.42	0.30	0.40
spectrum×10^{-4} /cm/s.s	0.40	0.41	0.42	0.33	0.55	0.58	0.53	0.44	0.43	0.18	0.44

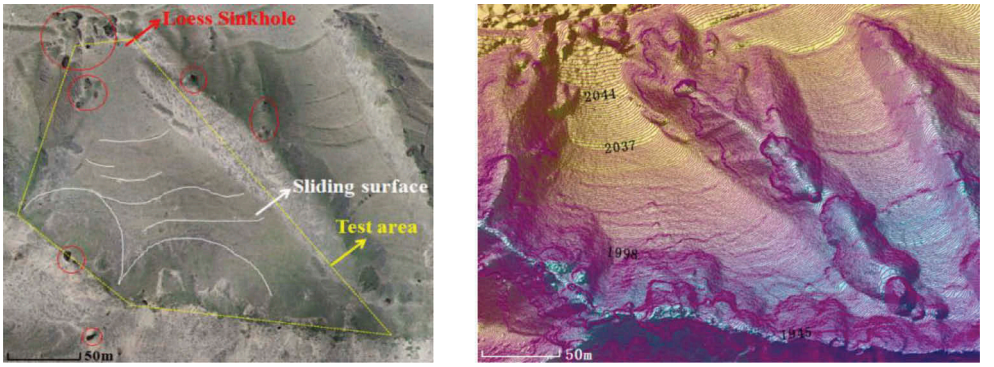

(a) Orthophoto data of the slope (b) Digital elevation information

Figure 5. Results of UAV aerial photography

slope elevation and slope is obtained, and the deformation characteristics of the slope are analyzed by the model.

4 COMPREHENSIVE ANALYSIS OF EARLY RECOGNITION

The microtremor is used to evaluate the dynamic amplification characteristics of the slope. On this basis, the method of Newmark sliding block was used to analyze the stability of the slope under the action of the Minxian-Zhangxian Ms 6.6 earthquake. In addition, using the data of the UAV, the deformation evolution characteristics of the slope were evaluated, and the sliding mode of the slope can be recognized.

4.1 *Analysis of the slope stability based on the dynamic amplification characteristic*

4.1.1 *Dynamic amplification characteristic of the slope*

Previous research reveals that the seismic wave field is amplified along the slope, and it is affected by the topographic features, the acceleration amplification alternates with the slope size (Song et al. 2017). The microtremor of the observation site is generated by various undirected sources, and various waves from all directions are randomly assembled. Assuming that it is a steady wave field, we define the value of the superior spectrum of each observation point divided by the superior spectrum at the foot of the slope as the amplification coefficient of the slope, as shown in the following formula:

$$A_n = \frac{(a_h)_n}{(a_h)_{10}} \tag{2}$$

where A_n= amplification coefficient; n=point 1, 2. . .11.

Based on the amplification coefficient of 11 observation points, the contour map is obtained using Kriging difference method, as shown in Fig. 6. It can be seen that the characteristics of dynamic amplification is amplified along the slope and related to the topographic features of the elevation and slope. The slope shows an amplification effect in the lower area of the slope where there are partial collapses, and the maximum reached 3.0 times.

4.1.2 *Analysis of the stability based on the method of Newmark sliding block*

Minxian-Zhangxian Ms 6.6 occurred on July 22, 2013 at Dingxi area (34.5°north latitude, 104.2°east longitude) in Gansu Province. The maximum ground motion was observed at Minxian station, which was 18 km from the epicenter, and the peak acceleration reached 220 gal, as shown in Fig. 7. Based on the distribution of the dynamic amplification characteristics

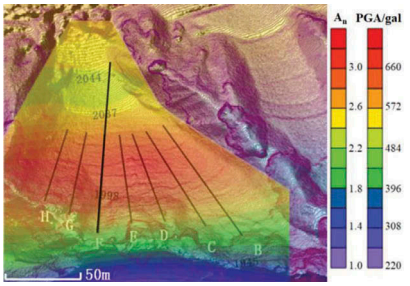

Figure 6. Distribution of amplification effect and acceleration under earthquake

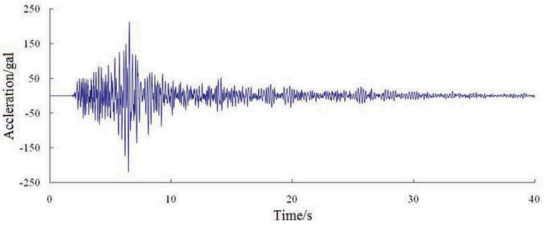

Figure 7. Acceleration characteristic of seismic wave

Table 2. Physical and mechanical parameters of loess in this region

Natural severity /(kN/m^3)	Cohesion /kPa	Internal friction angle/°
14.2	16.8	30.0

obtained from the microtremor, the distribution of acceleration under the seismic input of Minxian station was simulated. The peak acceleration of the slope reached 660 gal at the lower part of the slope, as shown in Fig. 6.

Considering the singularity of the loess slope material, the method of Newmark sliding block was used to calculate the stability. We introduced the ground motion inertial force, assumed that there was no saturated water layer in this slope, only considered the impact of the earthquake on the stability of the slope, and used formula (3), which was derived by Sun based on Newmark slider analysis method (Sun et al. 2011). In the formula, a is the average peak ground acceleration (PGA) of the calculation area, which was calculated from the amplification characteristic and monitoring data of the seismic station. Considering the result of the static calculation using PGA is too conservative, multiply the PGA by a factor of 0.65 as the a. $\beta$is the slope obtained by the digital elevation model. We also used the physical and mechanical parameters of loess in this region, which were obtained in the previous research of our group (Table 2) (Che et al. 2013).

$$F_s = \frac{g}{a}\left(\frac{\mathrm{c}}{\gamma h} + cos\beta\tan\varphi - sin\beta\right) \tag{3}$$

where F_s= factor of safety, c= cohesion, h= thickness of soil, γ= natural severity, β=slope, φ= internal friction angle, g= gravitational acceleration, and a=average acceleration, calculated by multiplying PGA by a factor of 0.65.

Then, we choose a typical profile F from the bottom to the top of the slope (as shown in Fig. 6) to obtain the terrain information. According to the terrain changes, the profile is roughly divided into six areas, as shown in Fig. 8. The safety factor of each area under earthquake action is calculated, the results are shown in Table 3, and the contour map is shown in Fig. 8.

The results show that in the area with large amplification effect, the safety factor is significantly reduced, and the characteristic of dynamic amplification strongly affects the slope stability. Therefore, it can be concluded that the area with a large amplification effect obtained by the microtremor has a risk of instability.

4.2 *Recognition of deformation*

To recognize the destroy mode of the slope, the deformation should be analyzed in detail. Considering the relative change of the study area, we select seven typical profiles (as shown in

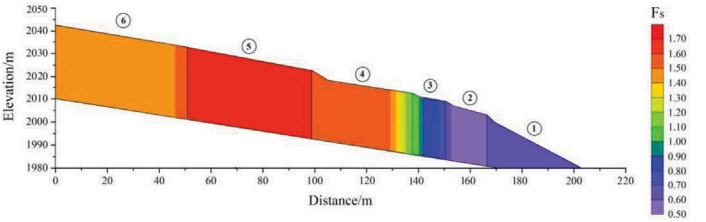

Figure 8. Division of areas and distribution of factor of safety

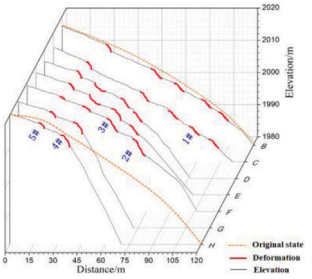

Figure 9. Profile data and deformations of the slope

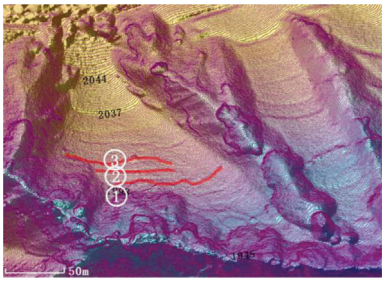

Figure 10. Results of early recognition

Table 3. Results of the safety factor

Number	Slope β/°	Thickness of soil h/m	Amplification coefficient A_n	PGA a/gal	Factor of safety F_s
1	21.81	33	2.36	338	0.64
2	20.94	33	2.77	397	0.59
3	18.44	33	2.32	332	0.86
4	7.95	33	2.27	325	1.50
5	9.09	33	1.95	279	1.66
6	7.67	33	2.45	351	1.40

Fig. 6) to analyze the deformation. The loess slope in this area has the characteristics of low vegetation coverage and flat surface topography, which are also observed from the orthophoto data. Using the relative deformation method to evaluate the deformation characteristics of the slope, we observe that there are many deformations in the surface of the slope, as shown in Fig. 9. Comparing with the image data, these deformations, which are at the same elevation, can be considered to have developed into connective trailing edges. The distribution of these trailing edges indicates that the trailing edges present a multilayered sliding mode.

4.3 *Results of recognition*

According to the analysis of the amplification effect obtained from the microtremor observation, the safety factor of areas 1, 2, and 3 in the lower part of the slope is less than 1.0 under earthquake; therefore, these areas have potential stability problems. Then, according to the results of deformation from the UAV aerial photography, there are several trailing edges in this area, which present a multilayered state, as shown in Fig. 10, and the sliding mode of the slope is recognized as multistage sliding. When the dynamic amplification characteristics and deformation characteristics are combined, the early recognition of earthquake landslide disasters can be achieved.

5 CONCLUSION

1. With the microtremor observation, the dynamic amplification characteristics of the slope can be evaluated; in combination with the analysis of stability under an earthquake, areas 1, 2, and 3 with large amplification effects are recognized as having a risk of instability.
2. Using the UAV aerial photography, the image data and digital elevation information can be obtained to analyze the deformation and sliding mode. The sliding mode of this slope is recognized as multistage sliding.
3. According to the analysis of stability based on the dynamic amplification and deformation characteristics, the early recognition of earthquake landslide disasters can be achieved.

ACKNOWLEDGEMENTS

This work is supported by the National Key R&D Program of China (2016YFC0803107-05). The authors would like to express their gratitude to Professor Ping Wang and Shaofeng Chai of the Key Laboratory of Loess Earthquake Engineering, CEA Gansu Province and Professor Fanyu Zhang of Lanzhou University for their helpful information provided.

REFERENCES

Alrawabdeh A., He F., Mousaa A., et al. 2016. Using an Unmanned Aerial Vehicle-Based Digital Imaging System to Derive a 3D Point Cloud for Landslide Scarp Recognition. *Remote Sensing*, 8 (2):95–127.

Che A.L., Wu Z.J. Peng D., Lei T., 2014. Surface Wave Investigation and Dynamic Stability Analysis for Earthquake-Induced Loess Landslides. *China Earthquake Engineering Journal*.35(4):724–729.

Huang R.Q., Xiang X.Q., 2004. Ju N.P. Assessment of China's regional geohazards: present situation and problems. *Geological Bulletin of China*,23(11):1078–1082.

Kritikos T., Davies T. 2015. Assessment of rainfall-generated shallow landslide/debris-flow susceptibility and run out using a GIS-based approach: application to western Southern Alps of New Zealand. *Landslides*, 12(6):1–25.

Pu X.W., Wang L.M. 2016. Engineering Geological Problem of Loess High Excavation Slope in Loess Hilly and Gully Region of Lanzhou and Its Stability Analysis. *China Earthquake Engineering Journal*, 38(5):787–794.

Roy R., Ghosh D., Bhattacharya G. 2016. Influence of strong motion characteristics on permanent displacement of slopes. *Landslides*, 13(2):1–14.

Sun Q., Zhang L., Ding X. L., et al. 2015. Slope deformation prior to Zhouqu, China landslide from InSAR time series analysis. *Remote Sensing of Environment*, 156:45–57.

Sun J.J., Wang L.M., Long P.W. 2011. An assessment method for regional susceptibility of landslides under coupling condition of earthquake and rainfall. *Chinese Journal of Rock Mechanics and Engineering*. 30(4):752–760.

Song D. Q., Che A.L., Zhu R.J., et al. Dynamic response characteristics of a rock slope with discontinuous joints under the combined action of earthquakes and rapid water drawdown. *Landslides*, 15(6): 1109–11250.

Turner D., Lucieer A., De Jong. S. M.2015.Time Series Analysis of Landslide Dynamics Using an Unmanned Aerial Vehicle (UAV). *Remote Sensing*, 7(2):1736–1757.

Xing A.G., Wu Z.J., Chen L.Z., Che A.L., Wang L.M. 2010. Characteristics of Secondary Typical Slope Disaster in Gansu Province Induced by the Wenchuan Earthquake. *Northwestern Seismological Journal*. 32(1):95–98.

Xu S.H., Wu Z.J. et al. 2013. Study of the Characteristics and Inducing Mechanism of Typical Earthquake Landslides of the Minxian-Zhangxian Ms6.6 Earthquake. *China Earthquake Engineering Journal*. 35(3):471–476.

Zhu R.J., Che A.L., Yan Fei, Wen Hai, Ge Xiurun. 2018. Research on dynamic evolution of rock slope with connective structural surface. *Rock and Soil Mechanics*,40(5):1–9.

Zhang X.C., Huang R.Q. 2014.Loess liquefaction characteristics and its influential factors of Shibeiyuan landslide. *Rock and Soil Mechanics*, 35(3):801–810.

Zhao W.C., Wu Z.J. 2016. Seismic Instability Mechanism of Landslide in the Loess Layer Based on Stress Analysis. *Journal of Catastrophology*. 31(4):224–228.
Zhang Q., Zhao C.Y. 2017. Semiautomatic Object-oriented Loose Landslide Recognition based on High Resolution Remote Sensing Images in Heifangtai, Gansu. *Journal of Catastrophology*. 32 (3):210–215.